Title

Kinetics of the catalytic cracking of naphtha over ZSM-5 zeolite: effect of reduced crystal size on the reaction of naphthenes

Authors

Hiroki Konno, Ryota Ohnaka, Jun-ichi Nishimura,

Teruoki Tago*, Yuta Nakasaka and Takao Masuda

Division of Chemical Process Engineering, Faculty of Engineering,

Hokkaido University, N13 W8, Kita-ku, Sapporo, Hokkaido 060-8628, Japan

** Corresponding author*

E-mail: tago@eng.hokudai.ac.jp

Tel: +81-117066551

Fax: +81-117066552

Keywords

Effectiveness factor; Thiele modulus; Mass transfer;

Catalytic cracking; Naphtha; Naphthene

Abstract

The catalytic cracking of model naphthenes (cyclohexane and methylcyclohexane) over ZSM-5 zeolites of different crystal sizes (macro and nanoZSM-5) was examined at reaction temperatures ranging from 748 to 923 K under atmospheric pressure, focusing on the associated reaction rate constants and activation energies. The catalytic cracking was found to follow first-order kinetics with respect to the naphthene concentrations and the activation energies for cyclohexane and methylcyclohexane cracking over nanoZSM-5 were determined to be 119 and 116 kJ/mol, respectively. In order to elucidate the rate-limiting step in the cracking process, the *Thiele modulus* and the effectiveness factor obtained from cracking over the two ZSM-5 zeolites were evaluated. Cracking with nanoZSM-5 proceeded under reaction-limiting conditions, whereas the reaction over macroZSM-5 at 923 K took place under transition conditions between reaction- and diffusion-limiting. The nanoZSM-5 was applied to the catalytic cracking of model naphtha and the results demonstrated that this catalyst was both effective and stable and generated a high yield of light olefins.

1. Introduction

Light olefins, such as ethylene and propylene, represent important feedstocks in the production of resins and other organic chemicals used in numerous industries, and the demand for these compounds continues to increase yearly.[1,2] Light olefins are typically produced by the steam cracking of naphtha, which gives ethylene and propylene yields of approximately 25 and 13%, respectively.[3-5] However, the amount of propylene which is currently generated by this process is insufficient to keep up with demand. To make up for this shortage, specially designed processes such as propane dehydrogenation and metathesis have been developed [6] although the output of these processes is also insufficient and accounts for only 2% of worldwide propylene production. Moreover, because steam cracking consumes more than 30% of the total amount of energy used in all petrochemical refinement processes, developing more efficient means for the production of light olefins is highly desirable.

In contrast, the catalytic cracking of naphtha over solid acid catalysts produces high propylene/ethylene ratios at low reaction temperatures and thus this process is expected to be an effective means of improving light olefins yield and saving energy when compared with steam cracking.[7-9] Zeolites have been identified as promising catalysts for the

catalytic cracking of naphtha and many studies concerning the catalytic cracking of C6-8 paraffins over zeolite catalysts have been reported.[10-16] However, the pore sizes of zeolites are almost equal to the molecular sizes of the hydrocarbons found in naphtha, and so one impediment to naphtha cracking is the restricted diffusion of these hydrocarbons within the zeolite channels. Moreover, since the crystal sizes of zeolites are usually much larger than the sizes of their micropores, the reaction rate tends to be limited by the diffusion of the reactant or product molecules within the micropores. One effective means of reducing the resistance to pore diffusion is to use nano-crystalline zeolites, [17,18] since the diffusion path length of hydrocarbon reactants and products depends on the zeolite crystal size, and thus is reduced in a nano-crystalline zeolite.[19-25]

Although naphthenes are important constituents of naphtha and affect the products generated from cracking, [26] few studies have been published concerning the cracking of naphthenes [27-32] compared to the quantity of papers which have been published on paraffin cracking. We believe that it is important to also investigate naphthene cracking in order to gain a better understanding of naphtha cracking. Currently, we are focusing on the catalytic cracking of naphthene over zeolite catalysts, [33] and have shown that ZSM-5 is an effective catalyst for naphthene cracking to generate light olefins.

In the present study, the kinetics of the catalytic cracking of two naphthenes (cyclohexane and methylcyclohexane) over ZSM-5 zeolite were investigated, using both the *Thiele modulus* and the effectiveness factor[34-37] to assess catalytic ability. The crystal size of the ZSM-5 zeolite necessary to achieve reaction-limiting conditions, in which the active sites within the zeolite are fully utilized during the cracking reaction, was also assessed. Finally, the catalytic cracking of model naphtha over ZSM-5 zeolites with different crystal sizes was carried out, and the effects of the crystal size on catalytic stability and light olefins yield were examined.

2. Experimental section

2.1 Zeolite preparation

Nano-crystalline ZSM-5 zeolite (nanoZSM-5) was prepared via hydrothermal synthesis using a water/surfactant/organic solvent mixture (the emulsion method).[38,39] An aqueous solution containing both a Si and Al source material was obtained by hydrolyzing each metal alkoxide in a dilute tetrapropylammonium hydroxide (TPAOH)/water solution. The water solution (10 ml) thus obtained was added to the surfactant/organic solvent (70 ml, surfactant concentration of 0.5 mol/l).

Poly-oxyethylene-(15)-oleylether and cyclohexane were employed as the surfactant and organic solvent, respectively. The resulting water/surfactant/organic solvent was poured into a Teflon-sealed stainless steel bottle and heated to 423 K for 72 h. In order to obtain macro-crystalline ZSM-5 zeolite (macroZSM-5), hydrothermal synthesis was also carried out, but without the surfactant/organic solvent, representing the conventional method. The precipitate thus obtained was washed with alcohol, dried at 373 K for 12 h and calcined at 823 K for 3 h in an air stream. Physically adsorbed and/or ion-exchanged sodium ions on the zeolite surface were removed and exchanged with NH_4^+ using a conventional ion exchange technique with a 10% NH_4NO_3 aqueous solution. The powdered NH_4^+-zeolite generated from the above process was pelletized, crushed and sieved to yield particles ca. 0.3 mm in diameter. The material was subsequently heated to 923 K to yield an H-ZSM-5 zeolite for the cracking reaction.

2.2 Characterization

The morphology and crystallinity of the obtained samples were analyzed using field emission scanning electron microscopy (FE-SEM; JSM-6500F, JEOL Co., Ltd.) and X-ray diffraction analysis (XRD; JDX-8020, JEOL Co., Ltd.), respectively. The

micropore volumes and the total and external surface areas of the samples were calculated using the BET- and *t*-methods based on N_2 adsorption isotherms (Belsorp mini, BEL JAPAN Co., Ltd.). The Si/Al ratios of the samples were determined based on X-ray fluorescence measurements (XRF; Supermini, Rigaku Co., Ltd.) and the acidity of the obtained samples was evaluated using the *ac*-NH_3-TPD method.[40] During the TPD measurements, the carrier gas was 1.0% NH_3 (balance He), the heating rate was 5 K min^{-1} and the temperature range was 373 to 823 K. The desorption of NH_3 molecules from the acid sites of the zeolite was measured under complete adsorption equilibrium conditions and the amount of NH_3 desorbed from the zeolite above 600 K was regarded as a measure of the number of strong acid sites.

2.3 Catalytic cracking

Cyclohexane (CH) and methylcyclohexane (MCH) were used as representatives of the naphthene fraction of naphtha. The cracking reactions of CH and MCH over ZSM-5 zeolite were carried out using a fixed-bed reactor at reaction temperatures of 748-923 K under N_2 at atmospheric pressure. Prior to each trial, a ZSM-5 zeolite sample was placed in a quartz tube reactor and activated at 923 K under N_2 flow for 1 h. Quartz tube reactors

with inner diameters of 4 or 10 mm were employed for the kinetics analysis and for the catalytic cracking of model naphtha, respectively. The *W/F* employed during these trials ranged from 1.28 to 5.11 kg mol^{-1} s^{-1} and the partial pressure of the reactant varied from 8.8 to 37 kPa at the inlet of the reactor. The composition of the exit gas was ascertained by on-line gas chromatography (GC-2014, Shimadzu Co., Ltd.), using a Porapak-Q column with a thermal conductivity detector (TCD) and Gaskuropack-54 and SP-1700 columns with a flame ionization detector (FID). N_2 was used as an internal standard during GC analysis with the TCD, during which the quantities of methane produced from cracking were quantified. Methane, ethylene, propylene and other hydrocarbon products were also quantified by GC analysis using the FID. The amount of coke deposited on the catalyst during each reaction was determined by thermogravimetric analysis (TGA; TGA-50, Shimadzu Co., Ltd.) under an oxygen/nitrogen atmosphere (oxygen: 10%) over the temperature range from 300 to 1173 K at a heating rate of 5 K min^{-1}.

2.4 Diffusivity measurement

The intracrystalline diffusivity and amounts of adsorbed CH and MCH within the

ZSM-5 zeolites in the vapor phase were measured by the constant volumetric method.[41,42] Assuming a zeolite crystal with a hexagonal slab shape, the uptake curve of the naphthene amount adsorbed within the zeolite crystal can theoretically be expressed by the following equation.

$$\frac{M_t}{M_e} = 1 - \sum_{n=1} \frac{2\alpha(1+\alpha)}{1+\alpha+\alpha^2 q_n^2} \exp\left(-\frac{Dq_n^2 t}{L^2}\right) \quad (1)$$

$$\text{where } \alpha = V/(\alpha_m WHL), \ \tan q_n = -\alpha q_n \quad (2)$$

Here, M_t is the amount adsorbed at time t, M_e is the value of M_t at equilibrium, D is the intracrystalline diffusivity, L is the half-thickness value of the ZSM-5 zeolite crystal, a_m is the external surface area of the zeolite crystal, W is the catalyst weight, V is the volume of the vapor phase and H is the partition factor, which is the ratio of the concentration of adsorbed molecules within the catalyst to that in the gas phase. The effective diffusivity, D_{eff}, which is usually used for the kinetics analysis of the overall reaction rate when employing the *Thiele modulus*, [34-37] is calculated by multiplying the intracrystalline diffusivity, D, by the partition factor, H. The details of the experimental apparatus and procedure are described in our previous papers.[41,42]

3. Results and discussion

3.1 Characterization

Figure 1 presents FE-SEM micrographs of the obtained macroZSM-5 and nanoZSM-5. These differently-sized ZSM-5 zeolites were obtained by the conventional and emulsion methods, respectively, and exhibited crystal sizes of approximately 2 μm and 100 nm. The X-ray diffraction patterns of these samples showed peaks consistent with those of an MFI-type zeolite. Table 1 summarizes the physicochemical properties of these two zeolites. While the external surface area was increased in the nano-sized zeolite crystal, both zeolites had the same micropore volume of 0.18 $cm^3\ g^{-1}$ and very similar BET surface areas, in the vicinity of 400 $m^2\ g^{-1}$. Additionally, the acid amounts estimated by *ac*-NH_3-TPD and the Si/Al ratios measured by XRF were almost the same regardless of crystal size. Further information concerning the detailed characterization of synthesized zeolites is provided in our previous papers.[24,33] Based on these data, we concluded that ZSM-5 zeolites having different crystal sizes had been obtained and these zeolites were then used as catalysts for the cracking reaction.

MCH cracking was conducted over these zeolites to determine their turn-over

frequency (TOF) values. Applying MCH partial pressures ranging from 12.7 to 30.0 kPa and a reaction temperature of either 823 or 873 K, MCH conversions less than 6% were obtained. The resulting TOFs measured during MCH cracking over the nano- and macroZSM-5 are listed in Table 1. Niwa and Katada have reported that the TOF obtained during catalytic cracking of a hydrocarbon correlates with the acidity (measuring both the strength and amount of acid sites) of the zeolite.[43,44] In this study, however, although the nano and macroZSM-5 zeolites had almost the same acidity, the TOF values measured during MCH cracking were evidently dependent on the crystal size of the zeolite, in which much higher TOFs were obtained from the nanoZSM-5. In order to elucidate the effect of crystal size on the catalytic cracking of MCH, the kinetics of the cracking reactions using both ZSM-5 zeolites were investigated.

3.2 Reaction kinetics

Under differential reaction conditions, the following expression holds true.

$$F_{A0}\triangle x_A / W = k_n \left\{C_{A0}(1-\triangle x_A / 2)\right\}^n \quad (3)$$

Here F_{A0} is the molecular flux of MCH, Δx_A is the conversion, W is the amount of catalyst, k_n is the reaction rate constant (under differential reaction conditions), C_{A0} is the initial concentration of MCH and n is the reaction order. The relationship between $F_{A0}\Delta x_A/W$ and $C_{A0}(1-\Delta x_A/2)$ obtained at 923 K is shown in Figure 2. As can be seen from this figure, the slopes are close to one regardless of the crystal size of the zeolite catalysts, and thus the catalytic cracking of MCH was first order with respect to the concentration. The same relationship between concentration and reaction rate was observed at all reaction temperatures, ranging from 748 to 923 K.

When the reaction is first-order, the following equation can be applied under an integral reaction condition;

$$W / F_{A0} = C_{A0} \int_0^{x_A} \frac{dx_A}{-r_A} = \frac{-\ln(1-x_A)}{kC_{A0}} \quad (4)$$

where k is the reaction rate constant under integral reaction conditions. The relationship between F_{A0}/W and $C_{A0}/-\ln(1-x_A)$ is shown in Figure 3, in which the slopes of the plots represent the reaction rate constant, k. The values of k thus determined are summarized in Table 2, demonstrating that the reaction rate constants for the catalytic cracking of MCH

at 923 K were 9.5 $\times 10^{-3}$ and 4.5 $\times 10^{-2}$ m^3 kg^{-1} s^{-1} when applying the macroZSM-5 and nanoZSM-5 zeolites, respectively.

The reaction rate constants for CH and MCH cracking were obtained in accordance with the above method at reaction temperatures ranging from 748 to 923 K and Figure 4 (a) presents the Arrhenius plots for the thermal and catalytic cracking of MCH. The reaction rate constants for catalytic cracking over the nanoZSM-5 zeolite were multiplied by the catalyst bed density (493 kg m^{-3}) to allow direct comparison of the reaction rate constants for thermal and catalytic cracking. The activation energy for catalytic cracking (116 kJ/mol) was much less than that associated with thermal cracking (280 kJ/mol), and the reaction rate constant for catalytic cracking was 2500 times larger than the rate of pyrolysis at 923 K. Therefore, naphthene cracking over ZSM-5 zeolite under mild conditions evidently provides advantages over the current industrial procedure employed during the thermal cracking of naphtha, which requires temperatures above 1073 K.

Figure 4 (b) shows the Arrhenius plots for MCH catalytic cracking over ZSM-5 zeolites with different crystal sizes. The reaction rate constants for *n*-hexane [25] and CH cracking over nanoZSM-5 zeolite are also included in this figure for comparison purposes. With regard to the nanoZSM-5 kinetics, the reaction rate constants for both naphthenes

CH and MCH cracking are almost the same, while the reaction rate constant for *n*-hexane cracking is much lower. The activation energies associated with the CH and MCH cracking reactions were 119 and 116 kJ/mol, both of which were slightly lower than the energy for the *n*-hexane cracking (126 kJ/mol). These results obviously indicate that naphthenes are more reactive than paraffins.

The reaction rate constant for MCH cracking over macroZSM-5 is also plotted in this figure. The reaction rate constant and activation energy obtained when using macroZSM-5 were both much lower than those measured when employing the nanoZSM-5. In the cracking reaction, the reactant molecules diffuse within the catalyst micropores to the acid sites on which the reaction takes place. Because the diffusion resistance of the reactant increases as the crystal size of the zeolite is increased, the diffusion of MCH within a ZSM-5 zeolite with a larger crystal size (the macroZSM-5) will affect the overall reaction rate constant, leading to an apparent dependency of the reaction rate constant on the crystal size. The evident differences in the activation energies between the nano and macroZSM-5 zeolites will be addressed further on.

The reaction rate constants during paraffin and naphthene cracking were quite different from one another. Moreover, the results demonstrated that the crystal size of the

zeolite affects the apparent reaction rate constant during MCH cracking, possibly due to the effects of a significant level of diffusion resistance. In order to design an optimal zeolite catalyst for naphtha cracking, it is therefore vital to investigate the reaction-limiting step for each reactant molecule.

3.3 Effectiveness factor and rate-limiting step

In order to investigate in detail the effects of crystal size on rate-limiting steps in the cracking reaction, both the *Thiele modulus* and the effectiveness factor associated with MCH cracking were calculated, using the reaction rate constant, k, shown in Table 2 and the effective diffusivity, D_{eff}. Because both the thermal and catalytic cracking of MCH occur at temperatures above 673 K, the effective diffusivity of MCH was measured using silicalite-1 (a MFI-type zeolite without Al) at 573 K. The effective diffusivity, D_{eff}, under the catalytic cracking conditions was estimated to be 4.1×10^{-12} m^2 s^{-1} based on the diffusivity of MCH within silicalite-1.

The relationship between the *Thiele modulus*, ϕ, and the effectiveness factor, η, was calculated according to the following equations.

$$\phi = \frac{V}{S}\sqrt{\frac{k \times \rho_{\mathrm{p}}}{D_{\mathrm{eff}}}} = L\sqrt{\frac{k \times \rho_{\mathrm{p}}}{D_{\mathrm{eff}}}}, \quad V = \frac{1}{2}S \times 2L \quad \text{in a slab-shaped crystal} \tag{5}$$

$$\eta = \frac{\tanh(\phi)}{\phi} \tag{6}$$

Here V, S, L and ρ_{p} are the volume, external surface area, half-thickness and density of the ZSM-5 zeolite crystal. The *Thiele modulus* and the effectiveness factor values for the reactions over the macroZSM-5 and nanoZSM-5 zeolites were calculated and the results are shown in Figure 5 and Table 3. The *Thiele modulus* and the effectiveness factor values associated with *n*-hexane and CH cracking were also calculated in the same manner and are also included in Figure 5 and Table 3.

When the *Thiele modulus*, ϕ, is less than 0.2, the effectiveness factor is above 0.99, indicating that the reaction proceeds under reaction-limiting conditions.[36,37] Since the effectiveness factor obtained for nanoZSM-5 was above 0.99 at 923 K when reacting each representative naphtha, it is evident that catalytic cracking with the nanoZSM-5 proceeded under reaction-limiting conditions.

The zeolite crystal size required to obtain a reaction-limiting process can be calculated by substituting a value of 0.2 for ϕ in Equation 5, with the results listed in Table 3. The calculated sizes show that *n*-hexane, CH and MCH cracking will proceed

under reaction-limiting conditions over a ZSM-5 zeolite (Si/Al = 200) with a crystal size below 90 nm. These results are in good agreement with the data obtained in our previous research, in which the application of nanoZSM-5 to the catalytic cracking of naphtha representatives was effective and gave light olefins with high yields while demonstrating stable activity.[33]

Because the cracking reaction over the nanoZSM-5 proceeded under reaction-limiting conditions, the reaction rate constant in Figure 3 is considered to equal the intrinsic reaction rate constant, and thus can be used to evaluate the *Thiele modulus* for the macroZSM-5, based on Equation 5. The macroZSM-5 crystal size was substituted into Equation 5, and the effectiveness factors for these zeolites were calculated, as presented in Table 3. Since the effective diffusivity of *n*-hexane within ZSM-5 zeolite is much higher than those of the naphthenes, the effectiveness factor for *n*-hexane cracking over macroZSM-5 was 0.65 (representing transition conditions), whereas the effectiveness factors associated with cracking of the naphthenes were both approximately 0.2 due to the correspondingly low diffusivities and large reaction rate constants. The effective diffusivity of each component (*n*-hexane, CH and MCH) in the zeolite pores was unchanged between the nano- and macroZSM-5 (Table 3). However, there are differences

in the diffusion resistance values, defined as L^2/D_{eff}, in which D_{eff} and L are the effective diffusivity and diffusion length (half-thickness or radius of the zeolite crystal), respectively. The diffusion resistance in the macroZSM-5 (L=1000 nm) was approximately 400 times larger than that in the nanoZSM-5 (L=50 nm). It has therefore been demonstrated that the cracking reaction over macroZSM-5 proceeded under transition and/or diffusion-limiting conditions.

The activation energies of MCH cracking over the macroZSM-5 and nanoZSM-5 zeolites were found to be 87 and 116 kJ/mol, respectively, as shown in Figure 4. Based on the above discussion, the difference in these apparent activation energies may be attributed to the rate-limiting step in MCH cracking when using nanoZSM-5 and macroZSM-5. When a first-order reaction proceeds under diffusion-limiting conditions, the apparent activation energy can be approximated by taking half of the intrinsic activation energy measured under reaction-limiting conditions, as in Equation 7.[36, 37]

$$E_{app} = \frac{E_{\text{int}}}{2} \quad \text{under diffusion-limiting condition} \tag{7}$$

Since the activation energy of MCH cracking over the nanoZSM-5 zeolite under

reaction-limiting conditions was 116 kJ/mol, the apparent activation energy under complete diffusion-limiting conditions is estimated to be 58 kJ/mol. The experimentally obtained activation energy of MCH cracking over macroZSM-5 was 87 kJ/mol, which is midway between the values for reaction-limiting conditions (116 kJ/mol) and diffusion-limiting conditions (58 kJ/mol). Because MCH cracking over macroZSM-5 proceeded under transition conditions, the diffusion of MCH within the macroZSM-5 will have a significant effect on the cracking reaction, and hence the apparent reaction rate constants and activation energies obtained when using macroZSM-5 were different from the values observed when employing the nanoZSM-5.

3.4 Catalytic cracking of model naphtha

The composition of a typical model naphtha is provided in Table 4,[45,46] in which the proportion of naphthene is approximately 20 mol%. As noted above, the macroZSM-5 exhibited a low effectiveness factor in naphthene (CH and MCH) cracking, whereas the cracking reaction occurred under reaction-limiting conditions over nanoZSM-5. Since naphtha is a mixture of alkanes, naphthenes and aromatics {benzene, toluene and xylene (BTX)}, the presence of naphthenes in naphtha are expected to affect both the product

selectivity and catalyst life time during naphtha cracking.

The effects of the zeolite crystal size on the catalytic cracking of model naphtha were also investigated using the macroZSM-5 and nanoZSM-5 zeolites, employing the model naphtha shown in Table 4 as the feedstock. The cracking reactions of the model naphtha over ZSM-5 zeolite were carried out using a fixed-bed reactor at a reaction temperature of 923 K under a N_2 flow at atmospheric pressure. The product distributions were ascertained by the same GC system as used during kinetic analysis, and were calculated based on the amount of hydrocarbon at the inlet of the reactor. Changes in the product yields and conversions of *n*-hexane and methylcyclohexane during naphtha cracking over the ZSM-5 zeolites are summarized in Figures 6 and 7, respectively.

A variety of products were obtained, including paraffins (methane, ethane, propane and butanes), olefins (ethylene, propylene and butenes) and aromatics. The olefins and aromatics were the major and terminal products, respectively, in naphtha cracking.

The macroZSM-5 exhibited a lower yield of olefins compared to the nanoZSM-5. Moreover, the product composition (Figure 6(a)) changed and the conversions of *n*-hexane and MCH (Figure 7(a)) decreased with time on stream during the naphtha

cracking; the proportion of aromatics decreased while the paraffins gradually increased, possibly due to catalyst deactivation during the cracking activity.

Because the cracking of paraffins (*n*-hexane) and naphthenes (MCH and CH) were found in the previous trials to take place under transition conditions over macroZSM-5 (as shown in Figure 5), the rate-limiting step in the cracking of each component of the model naphtha was associated with transition and/or diffusion-limiting conditions, in which the cracking reaction occurs on the acid sites near the external surface of the zeolite. During the cracking, both the reactants (alkanes and naphthenes) and products (olefins and BTX) are adsorbed on the pore walls and subsequently diffuse within the zeolite pore. In a multi-component diffusion system, as is the case with naphtha cracking, the hydrocarbon molecules with low diffusivities (naphthenes) inhibit the ability of the molecules with higher diffusivities (the linar alkanes and olefins) to diffuse out of the zeolite. Accordingly, the olefins generated under these conditions will encounter difficulty in diffusing out of the intracrystalline pores of the macroZSM-5, leading to long residence times of the olefins within the zeolite. Such prolonged residence times promote the formation of allyl carbenium ions by hydride transfer between the olefins and carbenium ions, leading to the generation of both BTX and coke. For these reasons, a

large amount of coke was deposited on the macroZSM-5 during the cracking (17.0 wt% after 260 min), resulting in gradual deactivation of the catalyst (Figure 7(a)).

In contrast, the nanoZSM-5 generated a greater proportion of light olefins (approximately 57 C-mol%) and exhibited more stable activity as compared with macroZSM-5 (Figure 7(b)). Because the cracking of the naphtha representatives took place under reaction-limiting conditions over nanoZSM-5, as shown in Figure 5, the cracking of each component in the model naphtha should take place under reaction-limiting conditions, in which the acid sites of the nanoZSM-5 located near the external surface as well as deep inside the crystal were fully used in the cracking reaction. Accordingly, a high olefins yield and stable activity resulted as shown in Figures 6(b) and 7(b), respectively. Moreover, the low diffusion resistance of reactants and products within the catalyst pores reduced the amount of coke deposited on the nanoZSM-5 during the cracking process (2.9 wt% after 260 min).

It is well known that Brønsted and Lewis acid sites exhibit different product selectivities in cracking reactions. Lewis acid sites may promote BTX and coke formation, resulting in the observed difference in the product distribution between macro- and nanoZSM-5, shown in Figure 6. Unfortunately, we were unable to obtain suitably clear

IR spectra of the macro- and nanoZSM-5 while using the pyridine adsorption method, due to the high Si/Al ratio in these materials. However, since the diffusion resistance of both reactants and products within the macroZSM-5 was approximately 400 times larger than in the nanoZSM-5, this difference in resistance presumably was the main factor affecting both the product distributions and the catalyst lifetimes. It is therefore apparent that the crystal size of the zeolite greatly affects the catalytic performance and that the application of nanoZSM-5 to the catalytic cracking of naphtha is an effective means of achieving the stable production of light olefins.

4. Conclusion

The catalytic cracking of methylcyclohexane (MCH) over ZSM-5 zeolite was examined. The reaction rate constants and activation energies associated with MCH cracking over both macroZSM-5 and nanoZSM-5 zeolites were determined, giving activation energy values of 87 and 116 kJ/mol, respectively. The reaction rate constants were applied to evaluate the effectiveness factor for MCH cracking over these ZSM-5 zeolites and the effectiveness factors for macroZSM-5 and nanoZSM-5 were calculated to be 0.21 and 0.99, respectively, at 923 K. The effectiveness factors in *n*-hexane and

cyclohexane for nanoZSM-5 and macroZSM-5 were also obtained. These kinetics data show that the cracking reaction over nanoZSM-5 proceeds under reaction-limiting conditions, and the crystal size of the ZSM-5 zeolite necessary to achieve reaction-limiting conditions was also clarified. Although naphthene encounters significant diffusion resistance within the zeolite crystal, this is dramatically reduced in smaller ZSM-5 crystals. The nanoZSM-5 thus exhibited high olefin yield and stable activity during naphtha cracking.

Acknowledgement

This work was supported by the Research Grant Program of the New Energy and Industrial Technology Development Organization (NEDO) of Japan.

References

1 O. Bortnovsky, P. Sazama, B. Wichterlova, *Appl. Catal. A: Gen*., 2005, **287**, 203.

2 C. Mei, P. Wen, Z. Liu, Y. Wang, W. Yang, Z. Xie, W. Hua, Z. Gao, *J. Catal.*, 2008, **258**, 243.

3 J. S. Jung, J. W. Park, G. Seo, *Appl. Catal. A: Gen*., 2005, **288**, 149.

4 T. Komatsu, H. Ishihara, Y. Fukui, T. Yashima, *Appl. Catal. A: Gen*., 2001, **214**, 103.

5 J. S. Plotkin, *Catal. Today*, 2005, **106**, 10.

6 T. Ren, M. Patel, K. Blok, *Energy*, 2006, **31**, 425.

7 Y. Yoshimura, N. Kijima, T. Hayakawa, K. Murata, K. Suzuki, F. Mizukami, K. Matano, T. Konishi, T. Oikawa, M. Saito, T. Shiojima, K. Shiozawa, K. Wakui, G. Sawada, K. Sato, S. Matsuo, N. Yamaoka, *Catal. Surv. Jpn.*, 2000, **4**, 157.

8 A. Corma, A. V. Orchillès, *Micropor. Mesopor. Mater.*, 2000, **35**, 21.

9 G. Wang, C. Xu, S. Gao, *Fuel Proces. Tech.*, 2008, **89**, 864.

10 P. Magnoux, P. Cartraud, S. Mignard, M. Guisnet, *J. Catal.*, 1987, **106**, 242.

11 A. Corma, V. Gonzàlez-Alfaro, A. V. Orchillès, *Appl. Catal. A: Gen*., 1995, **129**,

203.

12 A. Corma, F. V. Melo, L. Sauvanaud, F. Ortega, *Catal. Today*, 2005, **108-109**, 699.

13 H. Mochizuki, T. Yokoi, H. Imai, R. Watanabe, S. Namba, J.N. Kondo, T. Tatsumi, *Appl. Catal. A: Gen*., 2012, **449**, 188.

14 A. Corma, J. Mengual, P. J. Miguel, *Appl. Catal. A: Gen*., 2012, **421**, 121.

15 K. Urata, S. Furukawa, T. Komatsu, *Appl. Catal. A: Gen*., 2014, **475**, 335.

16 S. Inagaki, S. Shinada, Y. Kaneko, K. Takechi, R. Komatsu, Y. Tsuboi, H. Yamazaki, J.N. Kondo, Y. Kubota, *ACS Catal.*, 2013, **3**, 74.

17 L. Tosheva, V. P. Valtchev, *Chem. Mater.*, 2005, **7**, 2494.

18 S. C. Larsen, *J. Phys. Chem. C*, 2007, **111**, 18464.

19 S. Bao, G. Liu, X. Zhang, L. Wang, Z. Mi, *Ind. Eng. Chem. Res.*, 2010, **49**, 3972.

20 T. Wakihara, K. Sato, S. Inagaki, J. Tatami, K. Komeya, T. Meguro, Y. Kubota, *ACS Appl. Mater. Interfaces*, 2010, **2**, 2715.

21 T. Tago, H. Konno, M. Sakamoto, T. Masuda, *Appl. Catal. A: Gen*., 2011, **403**, 183.

22 H. Mochizuki, T. Yokoi, H. Imai, R. Watanabe, S. Namba, J. N. Kondo, T. Tatsumi, *Micropor. Mesopor. Mater.*,2011, **145**, 165.

23 A. A. Rownaghi, F. Rezaei, J. Hedlund, *Chem. Eng. J.*, 2012, **191**, 528.

24 H. Konno, T. Okamura, Y. Nakasaka, T. Tago, T. Masuda, *Chem. Eng. J.*, 2012, **207-208**, 460.

25 H. Zhang, Y. Ma, K. Song, Y. Zhang, Y. Tang, Journal of Catalysis, 2013, 302, 115.

26 P. B. Venuto, E. T. Habib, *Catal. Rev. Sci. Eng.*, 1978, **18**, 1.

27 A. Corma, A. Agudo, *Catal. Lett.*, 1981, **16**, 253.

28 A. Corma, F. Mocholi, V. Orchillès, *Appl. Catal. A: Gen.*, 1990, **67**, 307.

29 J. Abbot, B. Wojciechowski, *J. Catal.*, 1987, **107**, 571.

30 J. Abbot, *J. Catal.*, 1990, **123**, 383.

31 H. S. Cerqueira, P. C. Mihindou-Koumba, P. Magnoux, M. Guisnet, *Ind. Eng. Chem. Res.*, 2001, **40**, 1032.

32 A. Slagtern, I. M. Dahl, K. J. Jens, T. Myrstad, *Appl. Catal. A: Gen*., 2010, **375**, 213.

33 H. Konno, T. Tago, Y. Nakasaka, R. Ohnaka, J. Nishimura, T. Masuda, *Micropor.*

Mesopor. Mater., 2013, **175**, 25.

34 E.W. Thiele, *Ind. Eng. Chem.*, 1939, 31, 916.

35 R. Aris, *Ind. Eng. Chem. Fundamen.*, 1965, **4**, 227.

36 O. Levenspiel, *Chemical Reaction Engineering, 2nd ed., John Wiley & Sons,* 1972, 460.

37 H. S. Fogler, *Elements of Chemical Reaction Engineering, 4th ed., Prentice Hall*, 2006, 813.

38 T. Tago, M. Nishi, Y. Kouno, T. Masuda, *Chem. Lett.*, 2004, **33**, 1040.

39 T. Tago, H. Konno, Y. Nakasaka, T. Masuda, *Catal. Surv. Asia*, 2012, **16**, 148.

40 T. Masuda, Y. Fujikata, S. R. Mukai, K. Hashimoto, *Appl. Catal. A: Gen*., 1997, **165**, 57.

41 T. Masuda, *Catal. Surv. Asia*, 2003, **7**, 133.

42 T. Masuda, Y. Fujikata, T. Nishida, K. Hashimoto, *Micropor. Mesopor. Mater.*, 1998, **23**, 157.

43 K. Suzuki, T. Noda, N. Katada, M. Niwa, *J. Catal.*, 2007, **23**, 151.

44 M. Niwa, K. Suzuki, N. Morishita, G. Sastre, K. Okumura, N. Katada, *Catal. Sci. Technol.*, 2013, **3**, 1919.

45 A. Juarez, V. Macias, *Energ. Fuel*, 2000, **14**, 1032.

46 S.Y. Han, C.W. Lee, J.R. Kim, N.S. Han, W.C. Choi, C.H. Shin, Y.K. Park, *Stud. Surf. Sci. Catal.*, 2004, **153**, 157.

Captions

Figure 1. SEM micrographs of the (a) macroZSM-5 and (b) nanoZSM-5 zeolites.

Figure 2. Relationship between $F_{A0}\Delta x_A/W$ and $C_{A0}(1-\Delta x_A/2)$ in methylcyclohexane cracking over the macroZSM-5 (empty symbols) and nanoZSM-5 (filled symbols) zeolites.

Figure 3. Relationship between F_{A0}/W and $C_{A0}/-\ln(1-x_A)$ in methylcyclohexane cracking over the macroZSM-5 (empty symbols) and nanoZSM-5 (filled symbols) zeolites.

Figure 4. Arrhenius plots for (a) methylcyclohexane cracking over the nanoZSM-5 zeolite and (b) methylcyclohexane, cyclohexane and *n*-hexane cracking over the nanoZSM-5 and macroZSM-5 zeolites.

Figure 5. Relationships between the *Thiele modulus* and effectiveness factor for the methylcyclohexane, cyclohexane and *n*-hexane cracking reactions over the macroZSM-5 and nanoZSM-5 zeolites.

Figure 6. Product distribution obtained from catalytic cracking of model naphtha over the (a) macroZSM-5 and (b) nanoZSM-5 zeolites. Reaction conditions: T = 923 K, W/F = 0.25 h.

Figure 7. Conversions of *n*-hexane and methylcyclohexane during model naphtha cracking over the (a) macroZSM-5 and (b) nanoZSM-5 zeolites. Reaction conditions: T = 923 K, W/F = 0.25 h.

Table 1. Physicochemical characterization of the (a) macroZSM-5 and (b) nanoZSM-5 zeolites.

Table 2. Reaction order and reaction rate constant obtained with the ZSM-5 zeolites during methylcyclohexane, cyclohexane and *n*-hexane cracking at various temperatures.

Table 3. Intrinsic reaction rate constants, effective diffusivities and effectiveness factors for the *n*-hexane, cyclohexane and methylcyclohexane cracking reactions at 923 K over the macroZSM-5 and nanoZSM-5 zeolites.

Table 4. Composition of the model naphtha.

Figure 1

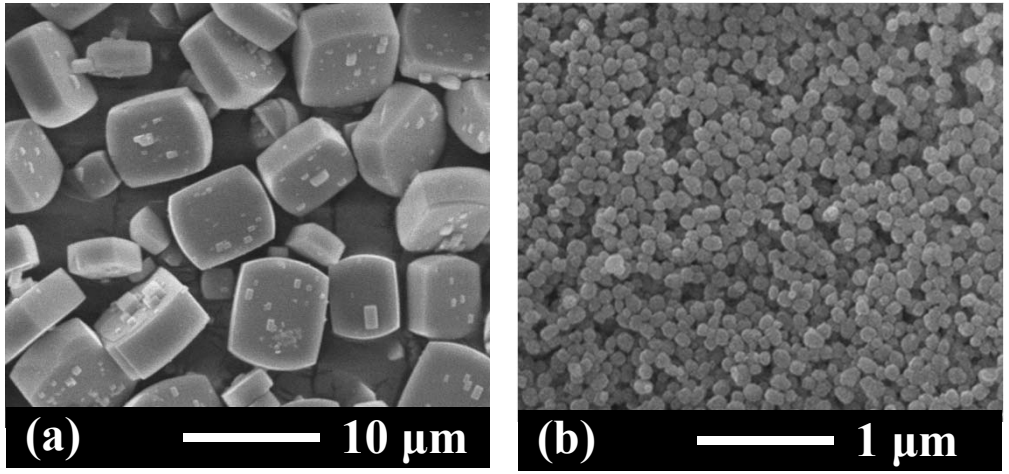

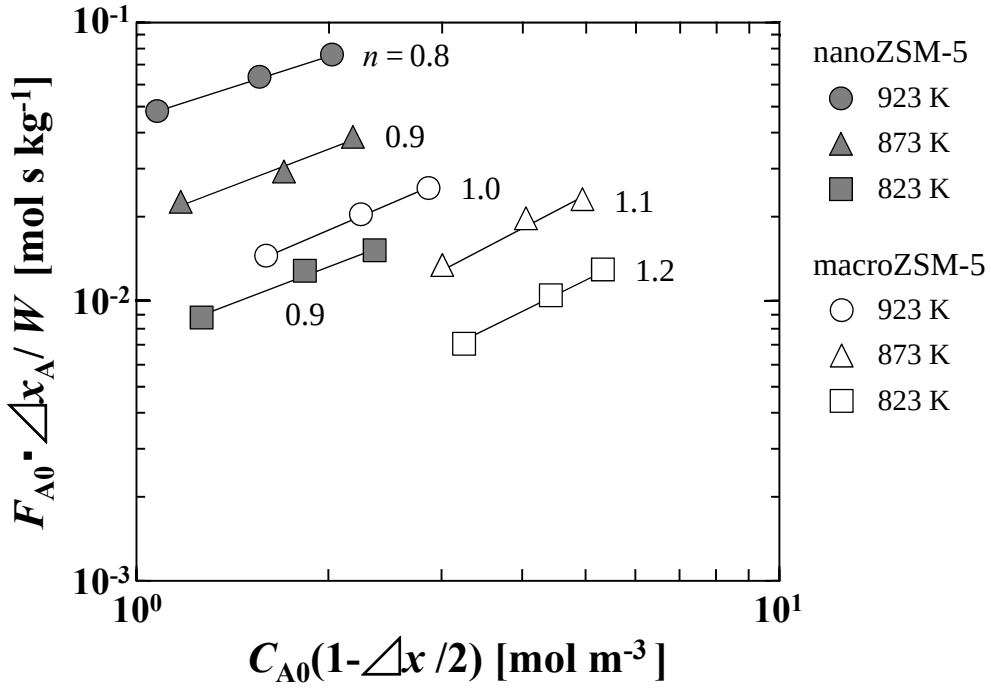
10^{-1}
10^{-2}
10^{-3}
10^{0}
10^{1}
$F_{A0} \cdot \Delta x_A / W$ [mol s kg^{-1}]
$C_{A0}(1-\Delta x/2)$ [mol m^{-3}]
n = 0.8
0.9
1.0
1.1
1.2
0.9
nanoZSM-5
923 K
873 K
823 K
macroZSM-5
923 K
873 K
823 K

Figure 3

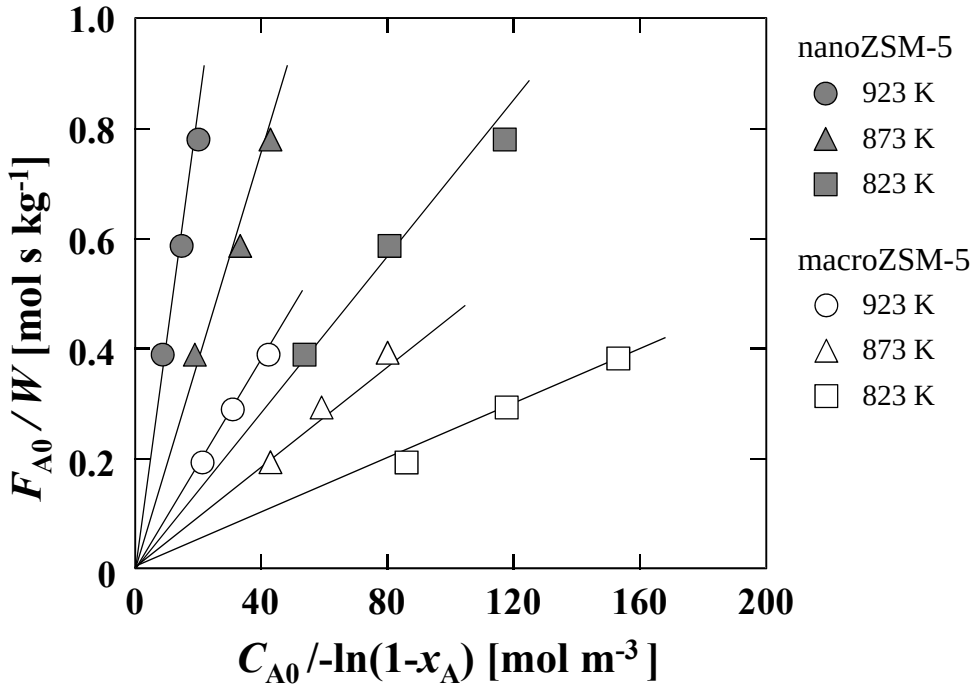
1.0
0.8
0.6
0.4
0.2
0
0
40
80
120
160
200
F_{A0} / W [mol s kg^{-1}]
C_{A0} /-ln(1-x_A) [mol m^{-3}]
nanoZSM-5
923 K
873 K
823 K
macroZSM-5
923 K
873 K
823 K

Figure 4

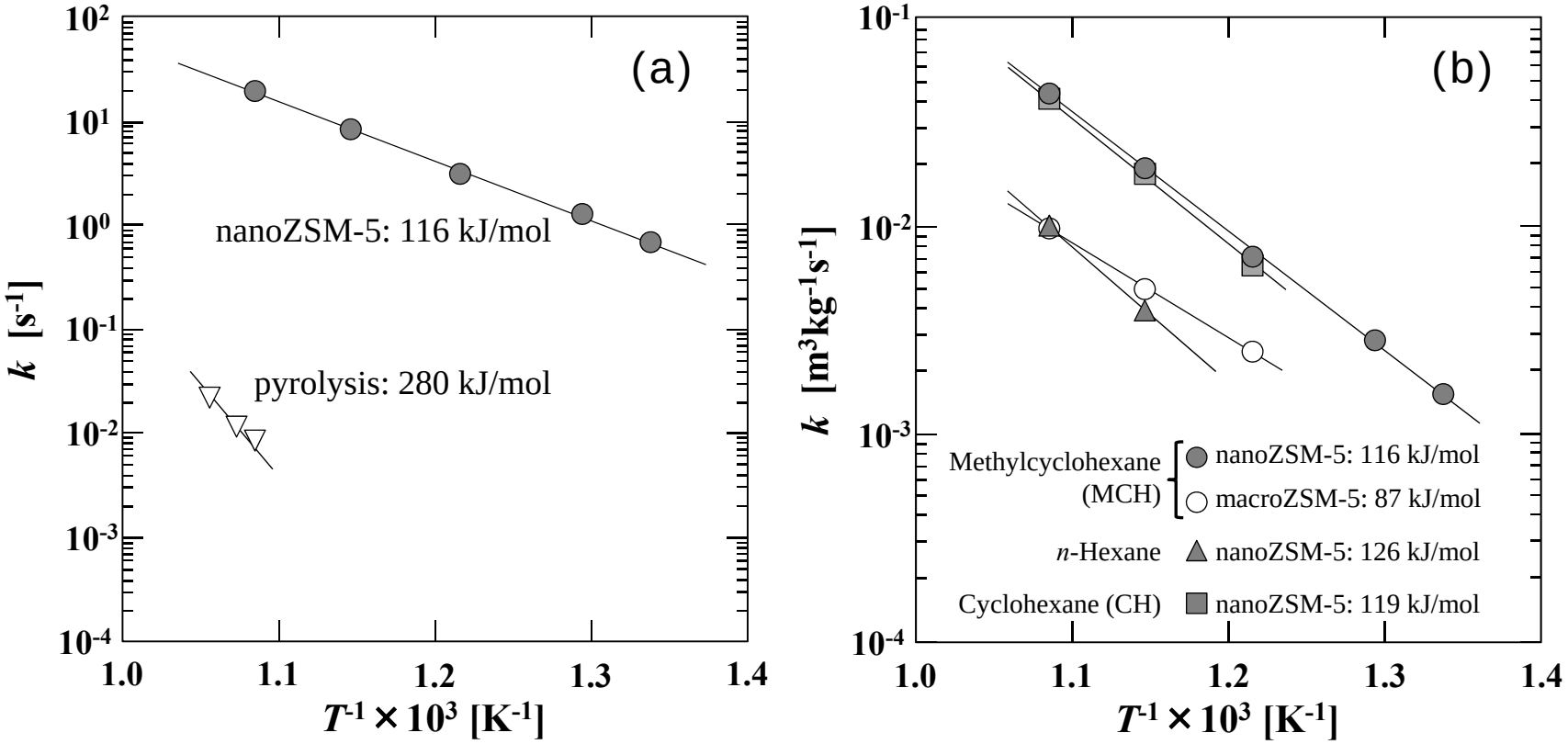
(a)
nanoZSM-5: 116 kJ/mol
pyrolysis: 280 kJ/mol
k [s-1]
T-1 × 103 [K-1]
(b)
Methylcyclohexane (MCH)
nanoZSM-5: 116 kJ/mol
macroZSM-5: 87 kJ/mol
n-Hexane
nanoZSM-5: 126 kJ/mol
Cyclohexane (CH)
nanoZSM-5: 119 kJ/mol
k [m3kg-1s-1]
T-1 × 103 [K-1]

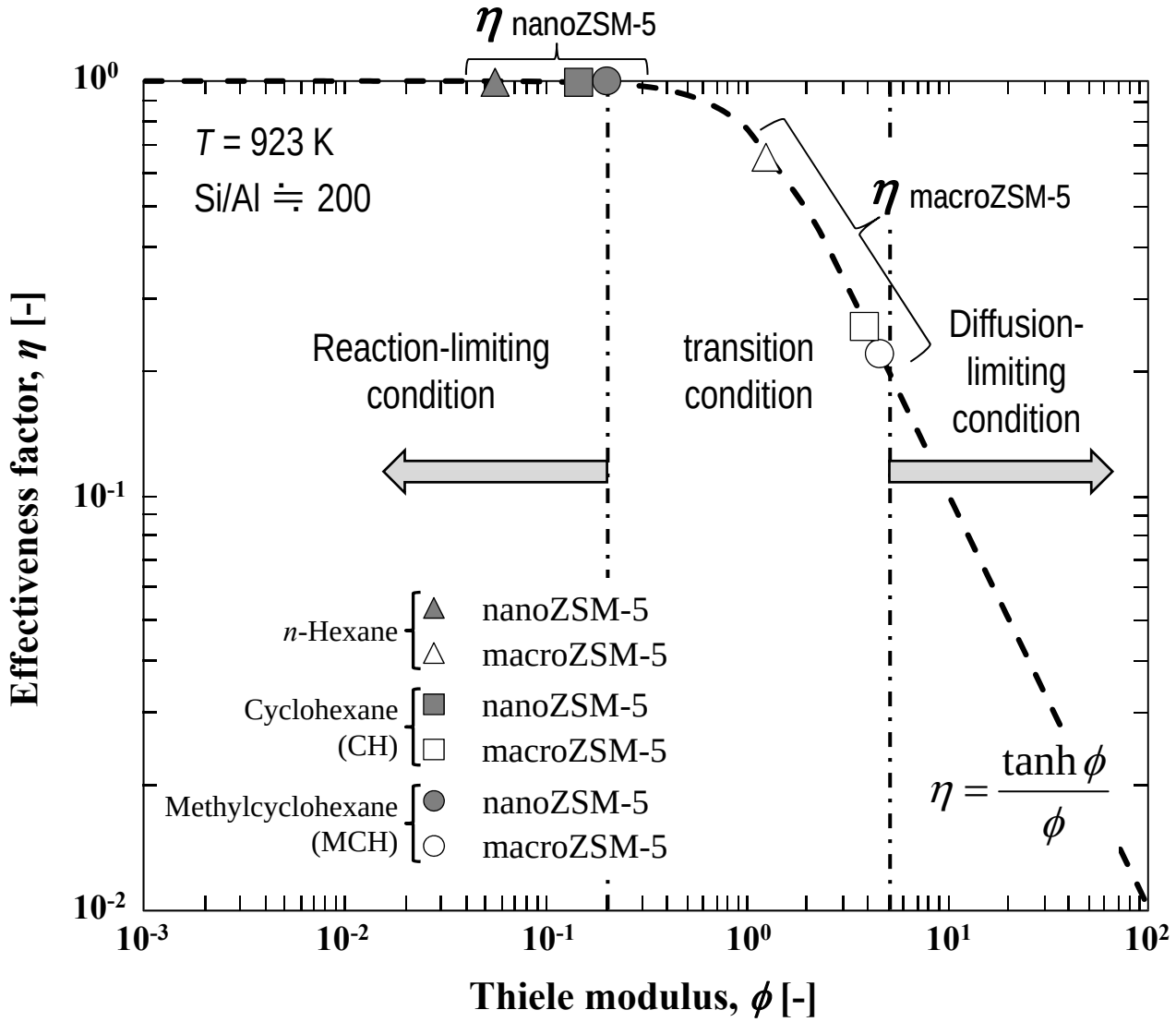
η nanoZSM-5
T = 923 K
Si/Al ≒ 200
η macroZSM-5
Reaction-limiting condition
transition condition
Diffusion-limiting condition
n-Hexane
nanoZSM-5
macroZSM-5
Cyclohexane (CH)
nanoZSM-5
macroZSM-5
Methylcyclohexane (MCH)
nanoZSM-5
macroZSM-5
η = tanh φ / φ
Effectiveness factor, η [-]
Thiele modulus, φ [-]
10^0
10^-1
10^-2
10^-3
10^-2
10^-1
10^0
10^1
10^2

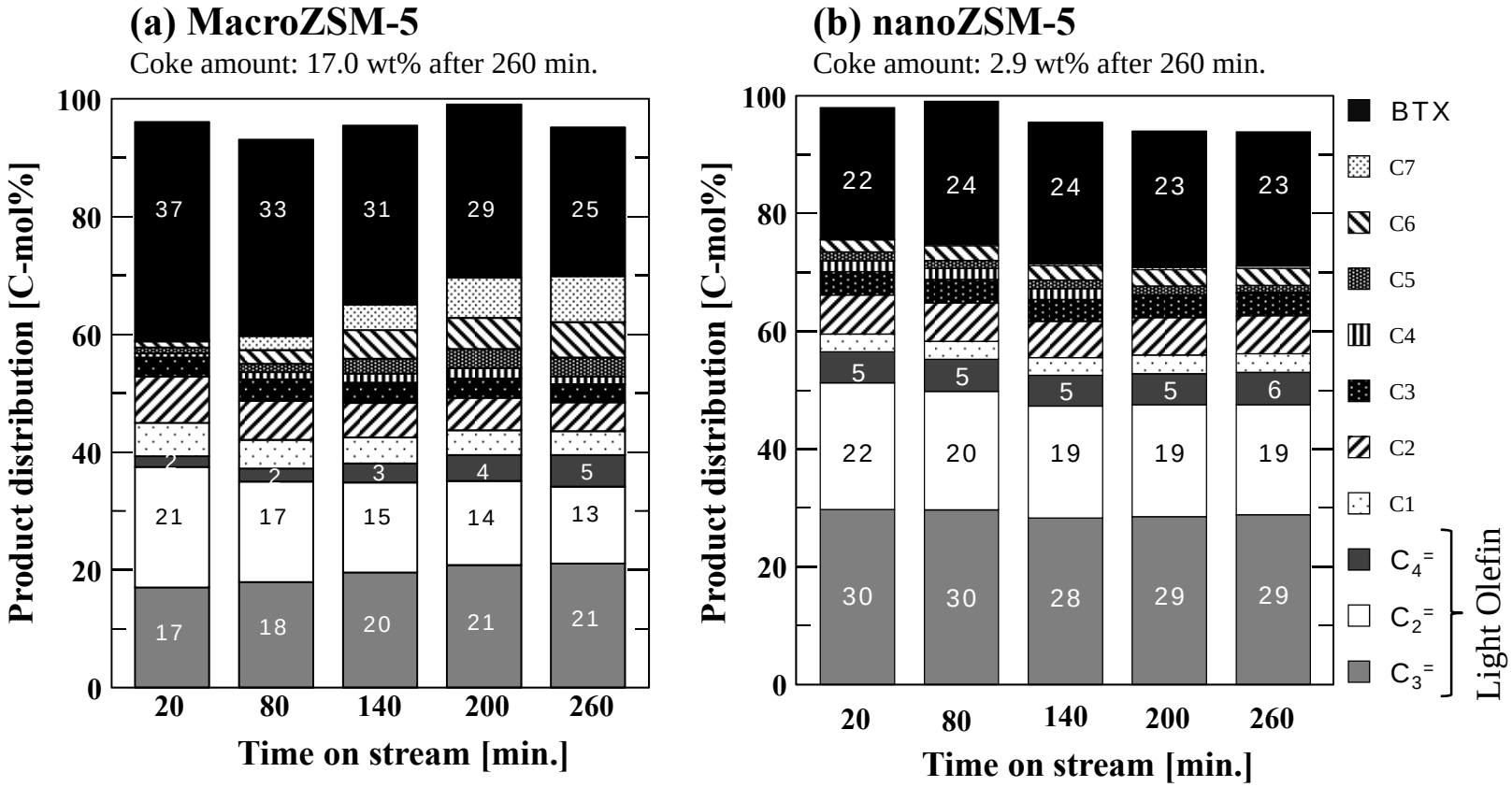
(a) MacroZSM-5
Coke amount: 17.0 wt% after 260 min.
(b) nanoZSM-5
Coke amount: 2.9 wt% after 260 min.
Product distribution [C-mol%]
Time on stream [min.]
20
80
140
200
260
0
20
40
60
80
100
37
33
31
29
25
2
2
3
4
5
21
17
15
14
13
17
18
20
21
21
22
24
24
23
23
5
5
5
5
6
22
20
19
19
19
30
30
28
29
29
BTX
C7
C6
C5
C4
C3
C2
C1
C4=
C2=
C3=
Light Olefin

Figure 7

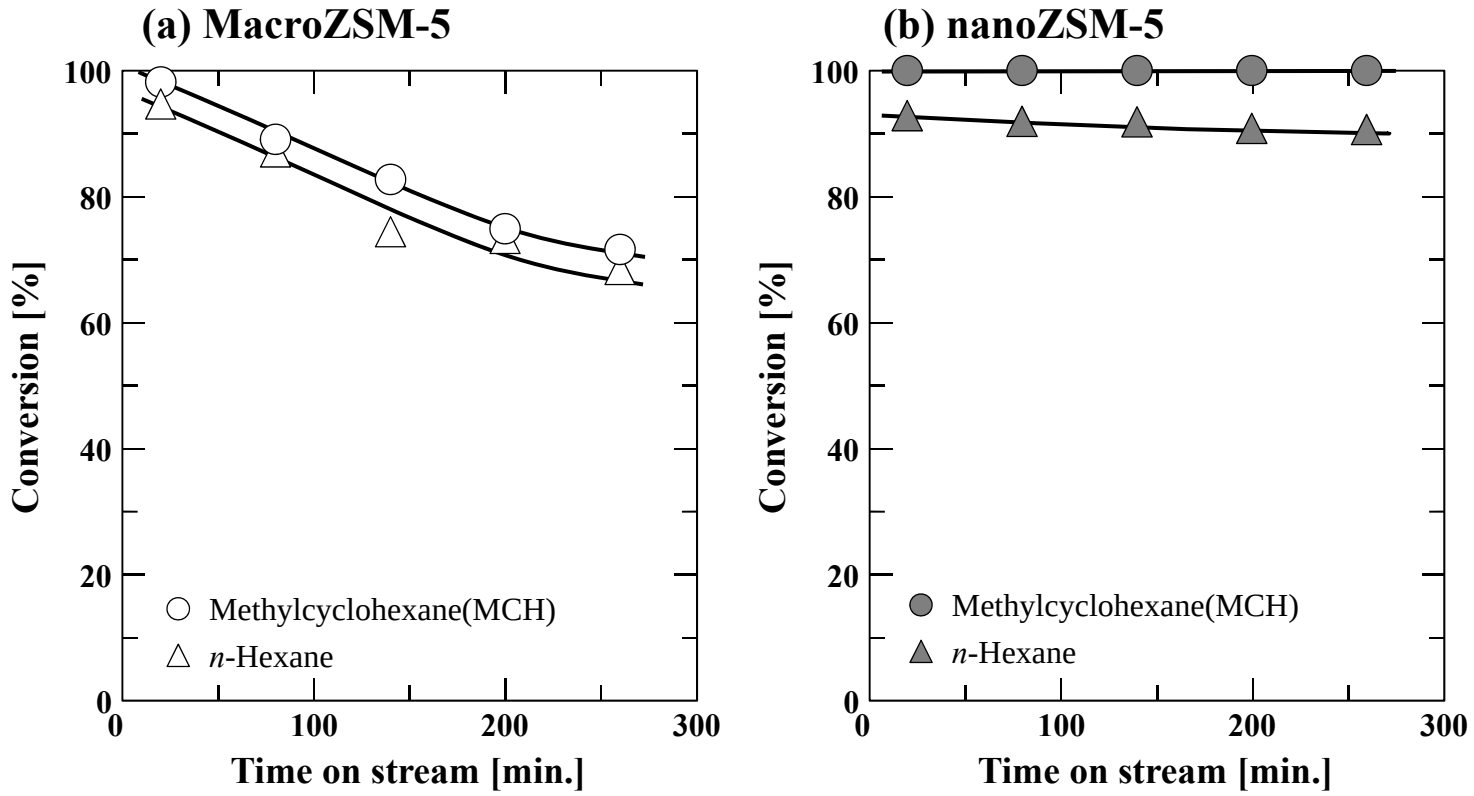
(a) MacroZSM-5
(b) nanoZSM-5
Conversion [%]
Time on stream [min.]
Methylcyclohexane(MCH)
n-Hexane
0
20
40
60
80
100
0
100
200
300

Table 1

zeolite catalyst	V_m [a] [cm^3g^{-1}]	S_{BET} [b] [m^2g^{-1}]	S_{EXT} [c] [m^2g^{-1}]	Si/Al [d] [-]	Acid amount [e] [mmol g^{-1}]	TOF for MCH cracking [s^{-1}] 823 K	873 K
nanoZSM-5	0.18	395	35	209	0.08	0.16	0.39
macroZSM-5	0.18	402	6	214	0.08	0.13	0.24

a Micropore volume
b BET surface area
c External surface area
d Atomic ratio of Si to Al measured by XRF
e Amount of strong acid sites estimated by *ac*-NH_3-TPD

Table 2

		reaction order n [a] [-]		reaction rate constant k [b] [m^3 kg^{-1} s^{-1}]	
	T [K]	nanoZSM-5	macroZSM-5	nanoZSM-5	macroZSM-5
methylcyclohexane	823	0.9	1.2	7.1×10^{-3}	2.4×10^{-3}
	873	0.9	1.1	1.9×10^{-2}	4.8×10^{-3}
	923	0.8	1.0	4.5×10^{-2}	9.5×10^{-3}
cyclohexane	823	0.9	-	6.5×10^{-3}	-
	873	1.0	-	1.8×10^{-2}	-
	923	1.0	-	4.3×10^{-2}	-
n-hexane	873	1.1	-	4.1×10^{-3}	-
	923	1.1	-	1.0×10^{-2}	-

a n: the slope of the plots in Figure 2
b k: the slope of the plots in Figure 3

Table 3

reactant	intrinsic reaction rate constant k_{int} [m^3 kg^{-1} s^{-1}] [a]	effective diffusivity D_{eff} [m^2 s^{-1}] [b]	effectiveness factor η [-] nanoZSM-5	effectiveness factor η [-] macroZSM-5	crystal size of zeolite required to achieve reaction-limiting condition [nm] [c]
n-hexane	1.0×10^{-2}	13.0×10^{-12}	1.00	0.65	340
cyclohexane	4.3×10^{-2}	4.8×10^{-12}	0.99	0.24	100
methylcyclohexane	4.5×10^{-2}	4.1×10^{-12}	0.99	0.21	90

a: reaction rate constant of nanoZSM-5 at 923 K
b: measured by constant volumetric method
c: by substituting 0.2 into ϕ in the equation (5)

Table 4

Average molecular weight [g/mol]	92.98
Density [g/cm^3]	0.722
Composition [mol%]	
n-hexane	20
3-methylpentane	20
n-heptane	15
n-octane	10
cyclohexane	10
methylcyclohexane	10
benzene	5
toluene	5
xylene	5